

# X-ray Čerenkov radiation. Theory and experiment

V. A. Bazylev, V. I. Glebov, É. I. Denisov, N. K. Zhevago, M. A. Kumakhov, A. S. Khlebnikov, and V. G. Tsinoev

*I. V. Kurchatov Institute of Atomic Energy*

(Submitted 15 May 1981; resubmitted 8 August 1981)

Zh. Eksp. Teor. Fiz. **81**, 1664–1680 (November 1981)

The real part of the permittivity is calculated on the basis of the Kramers-Kronig relation for frequencies close to the photoabsorption edge. It is shown that there exists a number of substances for which the permittivity exceeds unity in these frequency ranges. A theory of x-ray Čerenkov radiation is developed by taking into account the absorbing properties of the medium and the multiple scattering of particles. The results of an experimental investigation of Čerenkov radiation in carbon at frequencies close to the photoelectric-effect  $K$  edge are discussed.

PACS numbers: 78.70.En, 77.20.+y

## 1. INTRODUCTION

It is known that Čerenkov radiation from a charged particle is produced at a frequency  $\omega$  when the particle velocity  $v$  in a homogeneous medium exceeds the phase velocity  $[\epsilon'(\omega)]^{-1/2}$  of the light, where  $\epsilon'(\omega)$  is the real part of the permittivity of the medium.<sup>1</sup> The condition  $v > [\epsilon'(\omega)]^{-1/2}$  can usually be satisfied in the optical frequency region, where  $\epsilon'(\omega) > 1$ , for a large class of substances. Therefore most theoretical and experimental studies have been devoted to the properties of Čerenkov radiation in the optical band. The results of these investigations are reported in detail, for example, in the monographs of Jelley<sup>1</sup> and Zrelov<sup>2</sup> and in the review article by Bolotovskii.<sup>3</sup> A Stanford University group has recently succeeded in observing Čerenkov radiation of wavelengths down to 620 Å, produced in helium gas.<sup>4</sup>

It is usually assumed that Čerenkov radiation in the x-ray band is impossible in a homogeneous medium. What is meant here that  $\epsilon'(\omega)$  is less than unity at these frequencies and is of the form  $\epsilon'(\omega) = 1 - \omega_0^2/\omega^2$ , where  $\omega_0$  is the plasma frequency of the electrons of the medium. However, as shown by Kolpakov,<sup>5</sup> in a crystal having Mössbauer nuclei at the lattice sites, line, the positive contribution made to  $\epsilon'(\omega)$  by the interaction of the virtual photons with the nuclei can exceed near the nuclear transition line the negative contribution from the interaction with the electrons. In this case, the necessary condition for the Čerenkov radiation can be satisfied in quite narrow frequency intervals in the x-ray and  $\gamma$  bands.

Another possibility of Čerenkov radiation in the x-ray band was considered in detail in our preceding papers.<sup>6,7</sup> It was shown that allowance for the coupling of the electrons with the atoms of the medium alters the monotonic  $\epsilon'(\omega)$  dependence near the photoabsorption edges in such a way that for certain substances  $\epsilon'(\omega)$  can exceed unity. The predicted effect was recently observed in carbon at wavelengths  $\lambda \sim 40$  Å. The electron source was a beam from the linear electron accelerator of the Kharkov Physicotechnical Institute with electron energy 1 GeV. In this paper we report in detail the results of the theory of Čerenkov radiation in the x-ray band and compare the experimental data with the conclusions of the theory.

## 2. DISTINGUISHING FEATURES OF ČERENKOV X RADIATION FROM RELATIVISTIC PARTICLES

Although, as will be shown below, the permittivity in the x-ray band can indeed exceed unity, the deviation from unity, i.e., the susceptibility  $\chi'(\omega) \equiv \epsilon'(\omega) - 1$  turns out to be relatively small:  $\chi'(\omega) \ll 1$ . Therefore the particle threshold energy needed to generate the radiation turns out to be relativistic, and the radiation angles turn out to be small enough. In addition, the radiation is possible only in regions close to absorption lines and bands. In this case the theory used to describe the optical Čerenkov radiation becomes, generally speaking, inapplicable. A need arises for taking into account a number of effects connected with the rather large coherence length of the Čerenkov radiation.

The coherence length (formation length) of Čerenkov radiation can be calculated in the following manner. Let the electron move at constant velocity  $v$  and radiate a Čerenkov wave at a characteristic angle

$$\theta_0 = \arccos[1/v(\epsilon'(\omega))^{1/2}].$$

It is meaningful to speak of radiation if the wave lags the electron in the direction of its motion by a distance equal to the wavelength  $\lambda$ . During that time the electron negotiates a path equal to the coherence length  $l_{\text{coh}}$ . Since the wave velocity is  $(\epsilon'(\omega))^{-1/2}$ , the coherence length is determined by the relation

$$[v - (\epsilon'(\omega))^{-1/2}] l_{\text{coh}}/v = \lambda. \quad (1)$$

Therefore at small  $\chi' \ll 1$ , at ultrarelativistic velocities  $v \approx 1 - 1/2\gamma^2$ , and at small emission angles ( $\cos \theta_0 \approx 1 - \theta_0^2/2$ ) we obtain

$$l_{\text{coh}}(\omega) = \lambda/[\chi'(\omega) - \gamma^{-2}], \quad (2)$$

where  $\gamma$  is the Lorentz factor of the particle.

When the coherence length exceeds the photon absorption length  $l_c(\omega) = \lambda/\epsilon''$ , a more rigorous analysis of the radiation process becomes necessary.<sup>8</sup> Another possible factor that influences the process of formation of the Čerenkov radiation is multiple scattering of the radiating electrons.<sup>9–11</sup> The multiple-scattering effect can be estimated by replacing in (1) the particle velocity by its projection  $v \cos \theta_s$  on the direction of the initial motion,

where

$$\cos \theta_s \approx 1 - \theta_s^2/2, \quad \theta_s^2 = qL_{coh}, \quad q = E_s^2/(E^2L),$$

$q$  is the mean-squared multiple-scattering angle per unit path,  $E_s = 21$  MeV, and  $L$  is the radiation length of the medium. We find as a result that multiple scattering can be neglected if the multiple-scattering angle is smaller over the coherence length than the Čerenkov-radiation angle, i.e.,

$$(q/\omega)^{1/2}/[\chi'(\omega) - \gamma^2] \ll 1.$$

The foregoing qualitative arguments are confirmed also by more rigorous calculations.

### 3. THEORY OF ČERENKOV X-RADIATION IN AN UNBOUNDED ABSORBING MEDIUM

The classical Tamm-Frank equation for the spectral energy density of the Čerenkov radiation per unit time from a charge moving in an infinite absorbing medium is

$$d^2W/d\omega dt = e^2\omega(1-1/v^2\varepsilon'(\omega))\eta(v^2\varepsilon'(\omega)-1), \quad (3)$$

where  $\eta$  is the Heaviside function. At small  $\chi' \ll 1$  and at ultrarelativistic energies, Eq. (3) can be rewritten in the form

$$d^2W/d\omega dt = e^2\omega(\chi'(\omega) - \gamma^2)\eta(\chi'(\omega) - \gamma^2). \quad (4)$$

Budini<sup>1,2</sup> modified somewhat the Tamm-Frank result (3) to take absorption into account:

$$d^2W/d\omega dt = e^2\omega(1 - \varepsilon'(\omega)/v^2|\varepsilon(\omega)|^2)\eta(v^2\varepsilon'(\omega)-1), \quad (5)$$

where  $\varepsilon(\omega) = \varepsilon'(\omega) + i\varepsilon''(\omega)$  is the complex permittivity. In the case of interest to us  $|\chi| \ll 1$  and  $1 - v \ll 1$ , the Budini equation hardly differs from (4). Thus, the aforementioned absorption effect in the production of the radiation was not taken into account in the Tamm-Frank and Budini theories.

To take this effect into account, we use the general approach developed by Yakimets<sup>13</sup> and Zhevago<sup>14</sup> for the calculation of the energy losses of the particles in an absorbing medium. The spectral intensity density of the energy lost by the particle in an absorbing medium can be written in the form<sup>14</sup>

$$\frac{d^2W}{d\omega dt} = \frac{e^2\omega}{4\pi^4} \text{Im} \int \int L^{\mu\nu}(\tau, \mathbf{k}) D_{\mu\nu}(\mathbf{k}, \omega) d\tau d^3k, \quad (6)$$

where  $D_{\mu\nu}(\mathbf{k}, \omega)$  is the space-time Fourier component of the photon Green's function and  $L^{\mu\nu}(\tau, \mathbf{k})$  is the electron correlation-function tensor.

In the case of rectilinear motion, the following relation is valid

$$L^{\mu\nu} = v^\mu v^\nu e^{-i(\omega - \mathbf{k}\mathbf{v})\tau}, \quad (7)$$

where  $v^\mu$  are the components of the particle 4-velocity. For an isotropic medium, with a gauge having a zero scalar potential, the photon Green's function is of the form

$$D_{ik}(\mathbf{k}, \omega) = \frac{4\pi}{\omega^2\varepsilon(\omega) - k^2} \left( \delta_{ik} - \frac{k_i k_k}{k^2} \right) - \frac{4\pi k_i k_k}{\omega^2 k^2 \varepsilon_i(\omega, \mathbf{k})}, \quad (8)$$

where  $\varepsilon_i(\omega, \mathbf{k})$  and  $\varepsilon(\omega)$  are the longitudinal and transverse complex permittivities of the medium and  $\delta_{ik}$  is

the Kronecker symbol.

Substituting (7) and (8) in (6), we obtain

$$\frac{d^2W}{d\omega dt} = \frac{e^2\omega}{\pi^2} \text{Im} \int \delta(\omega - \mathbf{k}\mathbf{v}) \left[ \frac{v^2 - (\mathbf{k}\mathbf{v})^2/k^2}{\omega^2\varepsilon(\omega) - k^2} - \frac{(\mathbf{k}\mathbf{v})^2}{\omega^2 k^2 \varepsilon_i(\omega, \mathbf{k})} \right] \cdot d^3k. \quad (9)$$

The second term in the square brackets of (9) corresponds to the energy lost by the particle to excitation of longitudinal electromagnetic waves (plasmons). As  $\varepsilon_i'' \rightarrow 0$ , in particular, taking into account the relation

$$[\varepsilon_i(\omega, \mathbf{k})]^{-1} = \text{P.V.}[\varepsilon_i(\omega, \mathbf{k})] - i\pi\delta[\varepsilon_i'(\omega, \mathbf{k})]$$

we obtain a known result (see, e.g., Eq. (31.24) in Silin's monograph<sup>15</sup>) for the energy lost to excitation of weakly damped plasma oscillations. This part of the energy loss, however, has no bearing on the considered effects.

The energy lost by the particle on account of the interaction of the transverse part of the field with the medium is determined by the first term in (9). We choose an axis of the coordinate frame along the direction of the velocity  $\mathbf{v}$  in the space of the vectors  $\mathbf{k}$ . After integrating in (9) with respect to the modulus of the vector  $\mathbf{k}$  we obtain

$$\frac{d^2W}{d\omega dt} = \frac{e^2\omega v^2}{\pi} \text{Im} \int_0^\pi \frac{\sin^3 \theta d\theta}{\varepsilon(\omega)v^2 \cos^2 \theta - 1}. \quad (10)$$

In the limit of interest to us, Eq. (10) can be represented in the form

$$\frac{d^2W}{d\omega dt} = \frac{2e^2\omega}{\pi} \int_0^{\theta_m} \frac{\chi''(\omega)\theta^3 d\theta}{[\chi'(\omega) - \gamma^2 - \theta^2]^2 + [\chi''(\omega)]^2},$$

where the upper limit of integration with respect to the photon emission angles (which are generally speaking virtual) is given by

$$\theta_m = \min\{1, \omega^{-1}\}.$$

This choice of  $\theta_m$  corresponds to the employed approximation, wherein the dependence of  $\varepsilon$  on the momentum  $\mathbf{k}$  of the virtual photon is neglected. By the same token, no account is taken of the contribution made to the energy loss by the sufficiently close collisions of the particle with the atoms of the medium. This contribution should be calculated separately (see e.g., Ref. 16).

After integrating with respect to the photon emission angles relative to the particle-velocity direction, we obtain

$$\frac{d^2W}{d\omega dt} = \frac{e^2\omega}{\pi} \left[ \frac{\chi''(\omega)}{2} \ln \frac{\theta_m^4}{(\chi' - \gamma^2)^2 + (\chi'')^2} + (\chi' - \gamma^2) \left( \frac{\pi}{2} - \arctg \frac{\chi' - \gamma^2}{\chi''} \right) \right]. \quad (11)$$

Let us analyze the result. If the absorption of the virtual photons in the course of formation of the radiation is completely neglected ( $\chi'' \rightarrow 0$ ), we arrive at the Tamm-Frank result (4). In the other case, when the photon absorption over the coherence length is relatively small ( $\chi'' \ll |\chi' - \gamma^2|$ ) and the real part of the permittivity is negative ( $\chi'(\omega) = -\omega_0^2/\omega^2$ ) and Čerenkov radiation is impossible, we obtain

$$\frac{d^2W}{d\omega dt} = \frac{e^2\omega}{2\pi} \chi''(\omega) \ln \frac{\theta_m^4}{[(\omega_0/\omega)^2 + \gamma^2]^2}. \quad (12)$$

when  $\chi''(\omega)$  is determined by the photoabsorption by the atoms of the medium, Eq. (12) represents the spectral density of the energy lost by the particle to ionization. The quantity  $\omega$  is in this case the energy transferred by the particle to the atomic electron. If Eq. (12) is integrated with respect to  $\omega$  under the assumption that the logarithmic function changes little over the interval in which  $\chi''(\omega)$  changes substantially, we obtain the known Fermi result<sup>17</sup> for the ionization losses of an ultrarelativistic particle with allowance for the density effect:

$$\frac{dW}{dt} = -\frac{e^2 \omega_0^2}{2} \ln \left( \frac{1}{\omega_0} \right). \quad (13)$$

In the derivation of (13) we have used the Thomas-Reiche-Kuhn sum rule

$$\frac{2}{\pi} \int_0^\infty x \chi''(x) dx = \omega_0^2. \quad (14)$$

In the general case, when the length of formation of the Čerenkov radiation is comparable with the absorption length, the two terms in (11) are comparable in magnitude. In an unbounded absorbing medium, all the photons are sooner or later absorbed and the only observable effect is ionization and excitation of the atoms. In the general case it is impossible to distinguish uniquely between direct ionization and ionization due to absorption of Čerenkov radiation. On the other hand, if an attempt is made to measure the photon flux by some detector mounted inside the absorbing medium, the properties of the detector itself will influence substantially the spectrum of the registered radiation.

The difficulties connected with the separation of the energy losses into ionization and Čerenkov radiation can be eliminated by recording the photons behind a layer of material. The calculation of the radiation spectrum for this case will be carried out in Sec. 4 below.

When account is taken of multiple scattering of a particle, the picture of the radiation from a relativistic particle in an absorbing medium becomes even more complicated. The point is that multiple scattering cannot only influence the process of Čerenkov radiation, but is also a source of bremsstrahlung. This question was considered in detail by Bazylev, Varfolomeev, and Zherago.<sup>11</sup>

If no account is taken of the change of the rms multiple-scattering angle due to the energy lost by the particle, then the result for the spectral density of the energy lost by the particle per unit time can be represented in the form<sup>9,14</sup>

$$\frac{d^2W}{d\omega dt} = \frac{e^2}{\pi} (q\omega)^{1/2} F(s) + \frac{e^2 \omega}{\pi} (\chi' - \gamma^{-2}) \left( \frac{\pi}{2} + \arctg \frac{\chi' - \gamma^{-2}}{\chi''} \right) + \frac{e^2 \omega}{2\pi} \chi'' \ln \frac{\theta_m^4}{(\chi' - \gamma^{-2})^2 + (\chi'')^2} \quad (15)$$

$$F(s) = 4 \operatorname{Im} \left\{ s \left[ \psi \left( \frac{\beta}{2} \right) + \frac{1}{\beta} - \ln \frac{\beta}{2} \right] \right\} - 8\pi \eta (\chi' - \gamma^{-2} - \chi'') \operatorname{Re} \frac{s}{e^{i\pi\mu} - 1},$$

$$s = 1/2 (\gamma^{-2} - \chi) \left( \frac{\omega}{q} \right)^{1/2}, \quad \mu = 2s(1+i), \quad \beta = \mu \operatorname{sign} (\gamma^{-2} - \chi' + \chi''),$$

where  $\psi(x)$  is the logarithmic derivative of the  $\Gamma$  function, and  $q$  is the mean squared angle of multiple scat-

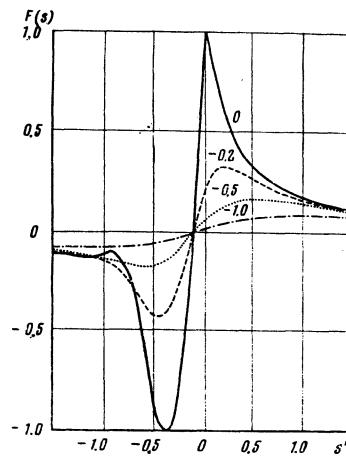


FIG. 1. Dependence of the function  $F(s)$  on the real part  $s'$  of the complex variable  $s$  at the values of  $s''$  indicated by the numbers on the curves.

tering of the particle on a unit path in the medium. The complex-variable function  $f(s)$  is represented by a set of plots in Fig. 1. Under the condition  $|s| \gg 1$ , the multiple scattering is insignificant, the first term in (15) is relatively small, and we obtain the previous result (11).

In the second case, when the absorption length greatly exceeds the radiation formation length, i.e.,  $|\operatorname{Re} s| \gg |\operatorname{Im} s|$ , the last term of (15) makes a negligibly small contribution, the second term can be represented in the form

$$e^2 \omega (\chi' - \gamma^{-2}) \eta (\chi' - \gamma^{-2}),$$

and the parameter  $s$  can be regarded as pure real. In this case relation (15) is the spectral distribution of the Čerenkov-radiation intensity, of the bremsstrahlung, and generally speaking, of their interference (in the region where  $-1 \lesssim s' \lesssim 0$ ). This result was also obtained by Pafomov<sup>10</sup> in an analysis of the spectrum of optical bremsstrahlung. The function  $\Phi(s)$  introduced by him is connected with  $F(s)$  for real negative  $s$ , by the relation

$$\Phi(s) = 2F(s)/\pi + 8s.$$

In the x-ray Čerenkov radiation case of interest to us, at frequencies close to the absorption lines and bands of the medium, the most substantial effect is absorption of virtual photons over the radiation-formation length, and the effect of multiple scattering can as a rule be neglected.

#### 4. ČERENKOV RADIATION GENERATED NEAR A BOUNDARY OF A MEDIUM

We calculate now the spectral distribution of the radiation energy that can be measured behind a layer of material in vacuum, when a charged particle passes through this layer. In this case the ambiguity connected with the separation of the contribution of the Čerenkov radiation to the ionization process is no longer present. However, the presence of a boundary medium leads to generation of transition x-radiation. As will be shown below, it is not always meaningful to consider these two types of radiation independently.

Since, as noted above, multiple scattering over the radiational-formation length can be neglected, it follows that the calculation of the radiation spectrum can be started with the known Garibyan formula<sup>18</sup> for the spectral-angular distribution of the radiation produced when a particle passes along a straight line through a plate of matter of thickness  $d$ . This equation is of the form

$$\frac{d^2 W}{d\omega d\Omega} = \frac{e^2}{\pi^2} \theta^2 |A(\omega, \theta)|^2, \quad (16)$$

$$A(\omega, \theta) = [(\gamma'^2 - \chi + \theta^2)^{-1} - (\gamma'^2 + \theta^2)^{-1}] \{1 - \exp[1/2 i \omega d (\chi - \gamma'^2 + \theta^2)]\}, \quad (16')$$

where  $\theta$  is the polar angle of the radiation,  $d\Omega \approx \theta d\theta d\varphi$  is the solid-angle differential, and  $\chi = \chi' + i\chi''$  is the complex permittivity.

Let the plate thickness exceed substantially the photon absorption length in the medium,  $d \gg l_c(\omega)$ . The exponential in (16') can then be neglected. Elementary integration of (16) over the radiation directions leads then to the following results for the spectral density of the radiation<sup>2)</sup> (Refs. 6 and 7):

$$\frac{dW}{d\omega} = \frac{e^2}{2\pi} \left\{ \left[ \left(1 - \frac{2\chi'}{\gamma^2 |\chi|^2}\right) \ln \frac{(\gamma'^2 - \chi')^2 + (\chi'')^2}{\gamma^{-4}} - 2 \right] + \frac{2}{\chi''} \left[ \chi' - \gamma'^2 - \frac{(\chi')^2 - (\chi'')^2}{|\chi|^2} \right] \left[ \frac{\pi}{2} + \text{arctg} \frac{\chi' - \gamma'^2}{\chi''} \right] \right\}. \quad (17)$$

In the frequency region where the real part of the dielectric susceptibility  $\chi'(\omega)$  is negative and the Čerenkov radiation is impossible, the second factor in the square brackets of (17) can be written in the form

$$\frac{\pi}{2} + \text{arctg} \frac{\chi' - \gamma'^2}{\chi''} = \text{arctg} \frac{|\chi'| + \gamma'^2}{\chi''}.$$

This case of transition radiation from an interface between an absorbing medium and vacuum was investigated in detail by Garibyan and Yang Shi.<sup>20</sup>

Let now the photon absorption length exceed substantially the formation length  $\chi'' \ll |\chi' - \gamma'^2|$ . Equation (17) takes then the form

$$\frac{dW}{d\omega} = e^2 \omega (\chi' - \gamma'^2) \eta (\chi' - \gamma'^2) l_c(\omega) + \frac{e^2}{2\pi} \left[ \left(1 - \frac{2}{\chi' \gamma'^2}\right) \ln \frac{(\gamma'^2 - \chi')^2}{\gamma^{-4}} - 2 \right], \quad (18)$$

where  $l_c = \lambda/\chi''$  is the photon absorption length. At relatively high frequencies when the plasma formula  $\chi'(\omega) = -\omega_p^2/\omega^2$  is valid, Čerenkov radiation is impossible [the first term in (18) is zero]. The second term in (18) coincides then with the known result<sup>21</sup> for the spectral energy distribution of the transition x-radiation. On the other hand, in the frequency region where  $\chi'(\omega)$  is positive, the second term in (18) can take on negative values (for example, at  $\chi' < 2/\gamma^2$ ), and then this term can no longer be regarded as the spectral density of the transition radiation. In this case it is more correct to speak of the influence of the boundary on the spectrum of the Čerenkov radiation [the first term in (18)], calculated by the Tamm-Frank formula (4) followed by allowance for the trivial absorption of the radiation along the path from the medium into the vacuum.

The considered example shows that x-ray Čerenkov and x-ray transition radiation can generally speaking not be considered independently. This holds in particular for the case when the formation length of the Čerenkov radiation is comparable in magnitude with the absorption length.

On the basis of an analysis of the general expression (17) it can only be stated that with increasing ratio

$$l_c(\omega)/l_{\text{coh}}(\omega) \sim (\chi' - \gamma'^2)/\chi''$$

towards positive values, the radiation comes closer in its properties to Čerenkov radiation, i.e., a noticeably pronounced generation threshold and a characteristic directivity along the generatrices of the cone appear (details follow). The significant role of the interference between the absorbing medium and the vacuum was noted also by Samsonov,<sup>22</sup> who investigated theoretically the structure of the radiation field.

## 5. CALCULATION OF THE PERMITTIVITY AND OF THE RADIATION SPECTRA

According to the results of quantum theory of photon scattering, the permittivity of a homogeneous medium can be expressed in terms of the amplitude of photons scattering through a zero angle by the atom of the medium (see, e.g., Ref. 23):

$$\chi(\omega) = \frac{4\pi n}{\omega} f(0),$$

where  $n$  is the number of atoms per unit volume. The imaginary part of the susceptibility determines the absorption of the photons and can be expressed, in accordance with the optical theorem, in terms of the absorption cross section  $\sigma^{(in)}(\omega)$  in the following manner:

$$\chi''(\omega) = n\omega^{-1} \sigma^{(in)}(\omega). \quad (19)$$

The real part of the susceptibility is connected with  $\chi''(\omega)$  by the Kramers-Kronig dispersion relation

$$\chi'(\omega) = \frac{2}{\pi} \int_0^\infty \frac{x \chi''(x)}{x^2 - \omega^2} dx. \quad (20)$$

Allowance for the interaction of the photons with the nuclei in the energy region close to the difference between the energy levels of the Mössbauer nuclei, can make the negative electron contribution to the real part of the permittivity smaller than the positive contribution from the interaction of the photons with the nuclei.<sup>5</sup>

We consider now the behavior of  $\chi'(\omega)$  near the edges of the electron photoabsorption of various shells of the atom. Relation (20) shows that electrons with binding energy exceeding the photon energy make a positive contribution to  $\chi'(\omega)$ . In the opposite case, the contribution turns out to be negative. The problem is to find media in which there exists an x-ray frequency region in which the positive contribution to  $\chi'(\omega)$  prevails over the negative contribution. In first-order approximation we can confine ourselves to the known form of the photoabsorption cross section  $\sigma^{(in)}(\omega)$  in the Coulomb approximation, and then calculate the integral in the right-hand side of (20). This calculation method was used, for example, by Hönl.<sup>24</sup> In the present case, however, it is not accurate enough. Since the photo-

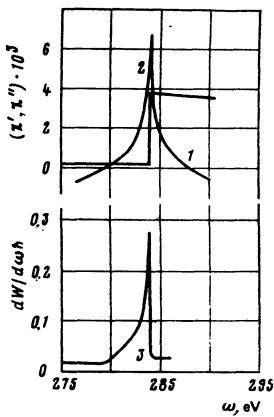


FIG. 2. Frequency dependence of the permittivity  $\chi'$  (curve 1),  $\chi''$  (curve 2), and of the spectral density of the radiation of electrons (3) with energy 1 GeV for carbon of density 1.0 g/cm<sup>3</sup>.

effect cross section changes jumpwise at the threshold,  $\chi'(\omega)$  has formally a discontinuity in such a calculation and one can arrive at the erroneous conclusion that a frequency region in which  $\chi'(\omega) > 0$  should exist in any medium near the photoabsorption edge. In fact, the photoeffect threshold is not abrupt. There exists a fine structure of the photoabsorption edges, due to the transitions of the electrons to valence levels. This structure must take into account in more accurate calculations of  $\chi'(\omega)$ .

We have performed such calculations by numerical methods with a computer. We used detailed experimental data on the photoabsorption cross sections as functions of the photon energy.<sup>25,26</sup> The lower and upper limits of the integrals in (20) were the first atom ionization threshold and the threshold of formation of electron-positron pairs, respectively. The test of the correctness of the calculations was simultaneous satisfaction of the sum rule (14). The calculated  $\chi'(\omega)$  for a number of media are shown by curves 1 in Figs. 2-4, together with the values of  $\chi''(\omega)$  (curves 2) in the frequency regions adjacent to the edges of the photoeffect on various shells. For the given number of media,  $\chi'(\omega)$  turned out to be positive in relatively narrow in-

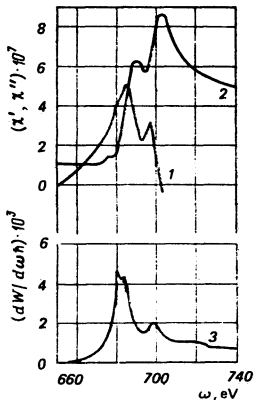


FIG. 3. Frequency dependence of the permittivity  $\chi'$  (curve 1),  $\chi''$  (curve 2), and of the spectral radiation density of electrons (3) with energy 1 GeV for xenon at a pressure 0.2 atm.

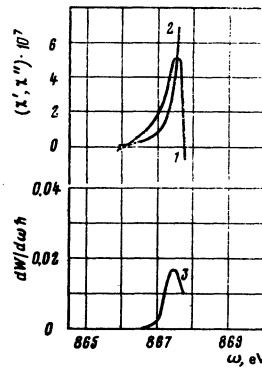


FIG. 4. Frequency dependence of the permittivity  $\chi'$  (curve 1),  $\chi''$  (curve 2), and of the spectral density of the radiation of electrons (3) with energy 1 GeV for neon at a pressure 1.0 atm.

tervals of the sought x-ray and of the vacuum ultraviolet frequency bands. On the other hand, in these frequency intervals the real part of the permittivity can greatly exceed its imaginary part. As shown above, this makes possible Čerenkov radiation in the indicated frequency intervals.

We calculated in accordance with (17) the spectral energy density of the radiation of an electron with energy 1 GeV, exceeding the threshold energy  $E_{th} = [\chi'(\omega)]^{-1/2}$  for all the substances given in Figs. 2-4 and a sufficiently large frequency interval. The results of the calculations are shown by curves 3 of these figures. In all the figures, the spectral density of the radiation energy has a clearly pronounced maximum whose position corresponds to and whose magnitude is proportion to the maximum of the ratio of the photon-absorption length to the coherence length.

## 6. SPECTRAL-ANGULAR DISTRIBUTION OF THE RADIATION

The spectral-angular energy density of the radiation from a sufficiently thick plate of material, without allowance for multiple scattering of the particles, is determined in accordance with (16) and (16') by the relation

$$\frac{d^2W}{d\omega d\Omega} = \frac{e^2}{\pi^2} \left| \frac{1}{\gamma^2 - \chi(\omega) + \theta^2} - \frac{1}{\gamma^2 + \theta^2} \right|^2 \theta^2. \quad (21)$$

The quantity (19), as function of the observation angle  $\theta$ , has generally speaking two maxima. The first corresponds to the Čerenkov emission angle

$$\theta_0(\omega) = (\chi'(\omega) - \gamma^{-2})^{1/2},$$

and the second to the transition radiation angle  $\theta_t = \gamma^{-1}$ . The relation between the values of these maxima depends on the ratio of the coherence length of the Čerenkov radiation to the photon absorption length.

If the coherence length of the Čerenkov radiation is small enough compared with the absorption length ( $\chi'(\omega) \gg \chi''(\omega)$ ) and the particle energy exceeds the threshold energy  $E_{th}$ , then at angles  $\theta$  close to  $\theta_0$  we can neglect the second term under the absolute value

sign in (21). As result we obtain

$$\frac{d^2W}{d\omega d\Omega} \Big|_{\theta=\theta_0} = \left(\frac{e}{2\pi}\right)^2 \frac{1}{[\theta-\theta_0(\omega)]^2 + [\chi''(\omega)/2(\chi'(\omega)-\gamma^{-2})^{1/2}]^2}. \quad (22)$$

Thus, Čerenkov radiation with a given frequency [such as to satisfy the condition  $\chi'(\omega) > \gamma^{-2}$ ] takes place in a narrow angle interval

$$\Delta\theta \approx \chi''(\omega) (\chi' - \gamma^{-2})^{-1/2}$$

around the angle  $\theta_0$ . The ratio  $\Delta\theta/\theta_0$  is equal, apart from a numerical factor, to the ratio of the coherence length to the absorption length.<sup>6,7</sup> At the same time, the value of the spectral-angular energy density of the radiation at the maximum (i.e., at  $\theta=\theta_0$ ) is proportional to the square of this ratio.

The real part of the susceptibility, shown in Figs. 2-4 as a function of  $\omega$ , has a maximum corresponding to the maximum Čerenkov radiation angle  $\theta_0^{(\max)} = (\chi'_{\max} - \gamma^{-2})^{1/2}$ . Owing to the relatively strong dispersion of  $\chi'(\omega)$  near the edges of the photoeffect, Čerenkov radiation with slightly different frequencies [within the limits of the region where  $\chi'(\omega) > \gamma^{-2}$ ] takes place at substantially different angles, from  $\theta_0^{(\max)}$  to zero angle. Each observation angle  $\theta$  corresponds to a certain radiation length with center at  $\bar{\omega}$ , determined from the relation

$$\chi'(\bar{\omega}) - \gamma^{-2} = \theta^2. \quad (23)$$

The shape and width of the line are obtained by expanding the denominator of (22) in powers of  $\Delta\omega = \omega - \bar{\omega}$ :

$$\approx \frac{1}{2} [\chi'(\bar{\omega}) - \gamma^{-2}]^{-3/2} \frac{d\chi'(\bar{\omega})}{d\bar{\omega}} \Delta\omega. \quad (24)$$

Thus, the line of emission by a single particle at an angle  $\theta$  as a Lorentz shape with a width

$$\Gamma(\bar{\omega}) = \frac{2\chi''(\bar{\omega})}{|d\chi'(\bar{\omega})/d\bar{\omega}|}. \quad (25)$$

Relations (24) and (25) are valid wherever  $\chi'(\omega) > \gamma^{-2}$ , with the exception of a certain vicinity of the maximum of  $\chi'(\omega)$ . Near this maximum, the expansion of  $\chi'(\omega)$  begins with terms quadratic in  $\Delta\omega$  and the line width turns out to be largest.

For a particle beam it is necessary to take into account also the inhomogeneous line broadening due to the scatter of the particles with respect to the angles at which they enter the target, and also due to their multiple scattering in the target. According to (23), the variations in the angles  $\theta$  between the direction of the particle velocity and the observation direction leads to variations of the line center

$$\Delta\bar{\omega} = \frac{\Delta(\theta^2)}{d\chi'(\bar{\omega})/d\bar{\omega}}.$$

Thus, relation (25) remains in force if the mean squared scatter of the particle angles and the mean squared angle of multiple scattering of the particles in the target are less than  $\Gamma(\omega)$ .

The spectral-angular distribution in (21) as a function of  $\omega$  is illustrated by a set of plots in Fig. 5, constructed for different observation angles  $\theta < \theta_0^{(\max)}$  of the Čer-

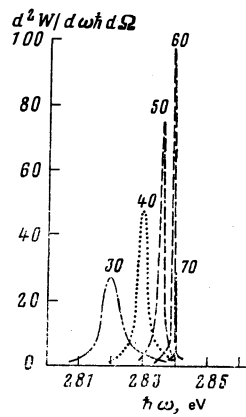


FIG. 5. Spectral-angular density of emission of electrons from carbon with  $\rho = 1.0 \text{ g/cm}^3$  vs. the photon energy for different observation angles. The numbers at the peaks denote the values of  $\theta$  in mrad.

enkov radiation in a layer of carbon with density  $\rho=1.00 \text{ g/cm}^3$  and with a thickness much larger than the absorption length. The electron energy was assumed to be 1.2 GeV.

## 7. EXPERIMENTAL OBSERVATION OF X-RAY ČERENKOV RADIATION

To check on the predictions of the theory, x-ray Čerenkov radiation in carbon was investigated. The work was performed with the LUÉ-2 linear electron accelerator of the Kharkov Physicotechnical Institute at an electron energy 1.2 GeV. Figure 6a shows the arrangement of the experimental setup. The electron beam (1) was accelerated, passed through a parallel-transport section, entered the experimental setup (2, 3) and proceeded further along an electron duct through a concrete shield to the next room. The experimental setup consisted of a special vacuum monochromator (2) built into one of the sections of the electron duct of the accelerator, a target unit, and a detector unit (3) located in a lead shield on the floor of the laboratory. Figure 6b

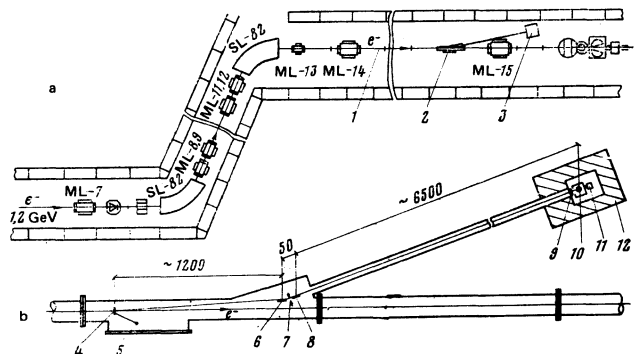


FIG. 6. Schematic diagram of experiment. a) Extraction of electron beam and location of experimental setup; b) arrangement of monochromator and of the detector unit; 1) electron beam; 2) monochromator; 3) detector unit; 4) target; 5) target rotation axis; 6) diffraction grating; 7) monochromator slit; 8) deflecting mirror; 9) metallic shutter; 10) proportional counter; 11) preamplifier; 12) lead shield.

shows the setup in a larger scale. The target (4) was suspended from thin holders and could be rotated about the axis (5) and removed from the electron beam for control measurements of the background produced by the electrons at the magnetic elements of the accelerator, at the collimators, and in the electron depth.

The target consisted of a plate of amorphous carbon with density  $1.75 \text{ g/cm}^3$ , transverse dimensions  $20 \times 56 \text{ mm}$  and thickness  $200 \text{ }\mu\text{m}$ . Two pieces of polyethylene film  $50 \text{ }\mu\text{m}$  thick, were fastened to the carbon plate on opposite sides in such a way that along one part of the target constituted successive layers of carbon and polyethylene, and the other layers of polyethylene and carbon. Since the radiation emerging from the target is actually picked off the last surface layer having a thickness on the order of the absorption length (several microns), it turned out that at an equal amount of matter on the path of the electrons it was possible to investigate the radiation from carbon of density  $1.75 \text{ g/cm}^3$  and polyethylene with a carbon-equivalent density  $0.83 \text{ g/cm}^3$ .

The monochromator operated at grazing incidence on a flat diffraction grating (6) having 1200 lines per millimeter. The angle of incidence of the radiation on the grating ranged from  $7$  to  $10^\circ$  when working in negative diffraction orders. To decrease the size of the monochromator and at the same time to locate the detector as far as possible from the electron beam, an additional deflecting mirror (8) was placed in the monochromator at a distance  $50 \text{ mm}$  from the diffraction grating behind a slit (7). The mirror was made of fused quartz. The angle of incidence of the radiation on the mirror was  $1.77^\circ$ . The total length of the monochromator turned out to be approximately  $7.6 \text{ m}$ .

The radiation detector was a cylindrical proportional counter (10) filled with  $90\% \text{ Ar} + 10\% \text{ CH}_4$  at a pressure  $0.10\text{--}0.15 \text{ atm}$ . The side window of the counter measured  $5 \times 20 \text{ mm}$  and was covered with a lavsan polyester film  $0.6 \text{ }\mu\text{m}$  thick, supported by a nickel screen with effective transmission  $50\%$ . Unfortunately the effective area of the inside working volume of the counter was 50 times larger than the area of the entrance window of the detector, so that the penetrating component of the background was registered by the entire working volume of the detector and the useful signals only by a small part of it. To measure the background of the hard electromagnetic radiation, a removable metallic shutter (9)  $1 \text{ mm}$  thick was installed ahead of the detector input window. The detector, the metallic shutter, and the detector preamplifier (11) were placed in a lead shield (12) on the floor of the laboratory at a distance of approximately  $2 \text{ m}$  from the electron duct of the accelerator. The length of the lead shield was  $40 \text{ cm}$  on the side of the input window of the detector and  $20 \text{ cm}$  on the other sides. The input opening in the lead shield had a diameter  $50 \text{ mm}$ .

The dimensions of the diffraction grating, of the deflecting mirror, and of the limiting diaphragms were such that it was possible to register events when the electron beam was shifted by  $\pm 7 \text{ mm}$  perpendicular to the dispersion plane of the grating. The elements of the monochromator and the target were placed in such a

way that the angle between the input axis of the monochromator and the axis of the electron beam was  $\theta_M = 8.42 \cdot 10^{-2} \text{ deg}$ .

On the basis of the calculations performed, Čerenkov x-ray photons should be observed at such an angle at a carbon-target density  $1.75 \text{ g/cm}^3$ . The shape of the photon spectrum under these conditions corresponds approximately to the curve shown in Fig. 5 for the angle  $\theta = 6 \cdot 10^{-2} \text{ rad}$ . It is seen that the radiation intensity has a clearly pronounced maximum with a peak width  $0.1 \text{ eV}$ . The monochromator was capable of an approximate energy resolution  $1 \text{ eV}$  for photons of  $300 \text{ eV}$  energy. In our measurements, however, owing to the instability of the electron beam, the energy resolution was decreased to  $50 \text{ eV}$ . The point is that the position of the electron beam in space during the experiment was shifted from the central position by as much as  $10 \text{ mm}$ . Since a  $\sim 50 \text{ eV}$  displacement of the emission point in the dispersion plane led to a shift of the detection region in the energy spectrum of the photon, it made no sense to tune the monochromator to a higher energy resolution. Installation of an input diaphragm, i.e., operation with a fixed angle of incidence of the radiation in the diffraction grating, would make it possible to operate with a higher energy resolution of the monochromator, but then the radiation source would turn out to be "blinking" and normalization of the results would be impossible. The solid angle subtended by the monochromator was  $10^{-6} \text{ sr}$ .

The LUÉ-2 accelerator operated in a pulsed regime with an electron pulse duration  $1.2 \text{ sec}$  and a frequency  $50 \text{ Hz}$ . The counting rate of the detector phonon signals, which coincided in time with the accelerator pulse, depended on the electron current. At an average current larger than  $10^{-6} \text{ A}$ , the counting rate of the detector was practically  $50 \text{ Hz}$  and in this regime it was impossible to note the addition of the useful signals. The electron current was chosen to be such that the frequency of the appearance of the phonon count with the counter window closed did not exceed  $10 \text{ Hz}$ . At total counting rates less than  $10 \text{ Hz}$ , under the given conditions, the useful-signal counting rates combined practically linearly with the phonon-signal counting rate. The optimal average electron current was  $10^{-7} \text{ A}$ . The accelerator current was measured with secondary emission monitor SEM, located  $5.5 \text{ m}$  away from the monochromator. In front of this monitor was placed a second monitor SEM<sub>2</sub> with an opening for the electron beam passing along the electron-duct axis. When the electron beam was deflected away from the electron-duct axis, the counting rate of the second monitor SEM<sub>2</sub> increased and the counting rate of the first monitor SEM<sub>1</sub> decreased. Therefore the test of the stability of the position of the electron beam in space during the described measurement was the ratio  $N(\text{SEM}_1)/N(\text{SEM}_2)$  of the counts. The same test was used when the beam of the electron was passed through the electron duct. The phonon counting rate of the detector decreased at the maximum ratio of  $N(\text{SEM}_1)$  to  $N(\text{SEM}_2)$ .

We measured the spectrum of the radiation of the electrons from the carbon target of density  $1.75 \text{ g/cm}^3$ . To

decrease the influence of the instability of the position of the electron beam on the target, the measurements were performed in short runs of 100 sec each. We measured the difference between the counting rates of the detector with the input window of the counter opened and closed, as a function of the rotation angle of the diffraction grating, i.e., scanning was carried out over the spectrum. The recorded number of events was normalized in each measurement to the corresponding value of the electron current against the monitor SEM<sub>1</sub>. The effect was 5–7% of the background level. Any run in which the ratio  $N(\text{SEM}_1)/N(\text{SEM}_2)$  with the detector input window closed differed from the ratio with the counter window open by more than 5% was discarded.

The measurement results are shown in Fig. 7. Several intensity peaks are seen in the spectrum of the diffracted photons. The diffraction orders labeled  $m_m$  correspond to travel of the rays in the monochromator from the target to the detector through the diffraction grating and next through the slit and the deflecting mirror. The diffraction orders labeled  $m_r$  correspond to the possible path of the rays from the target to the detector, with the deflecting mirror bypassed. The latter ray path was made possible by decreasing the energy resolution of the monochromator from 1 to 50 eV, for which purpose it was necessary to open the slit (7) to a width of 1 mm. In this case the diffraction condition started to be satisfied for the diffraction-grating farthest from the target, and we observed a double pattern of peaks. These peaks belonged to different orders of diffraction of photons with energy 284 eV. Since the energy resolution did not make it possible to determine exactly the photon energy, the results of the measurements (Fig. 7) made it impossible to state with sufficient reliability that it was precisely 284-eV Čerenkov radiation which was observed rather than, for example, the characteristic carbon  $K\alpha$  line with energy 277 eV, excited by the electrons. A control experiment was

therefore performed with the target, in which the last material transversed by the beam was polyethylene and not carbon. The maximum calculated Čerenkov-cone angle turned out to be in this case smaller than the observation angle  $\theta_M$ , and the detector should therefore not have registered the Čerenkov photons from the polyethylene. Estimates show that the characteristic radiation was the same for both targets, since it should not have depended substantially on the density of the medium. On the other hand, no peaks was observed in the spectrum measured with the polyethylene target (see histogram 2 of Fig. 7), while the peaks due to the carbon target had a clearly pronounced character. This fact by itself, without measuring the absolute intensity, can be attributed only to Čerenkov radiation which, in contrast to the characteristic radiation, has a specific angular directivity (see Sec. 6 above). Performance of absolute measurements of the radiation intensity from the target calls for knowledge of the efficiency of the reflection of the photons by the diffraction grating and by the deflecting mirror directly in the course of the experiment. No such measurements were made, so that it is difficult to cite the absolute values of the intensity of the Čerenkov radiation in this experiment.

From the measurement of the maximum angle of the Čerenkov radiation, using Eq. (23), it is possible to calculate the maximum value of the real part of the permittivity near the photoabsorption  $K$  edge of carbon. Since Čerenkov radiation from carbon of density  $\rho=1.75$  g/cm<sup>3</sup> enters into a monochromator set at an angle  $\theta_M=8.42 \cdot 10^{-2}$  rad to the electron-beam axis, while the radiation from polyethylene does not, we can estimate the limits of the maximum angle of the Čerenkov radiation from carbon:

$$\theta_{\text{CH}_2} < \theta_M \leq \theta_C.$$

From this we obtain for carbon with a reduced density  $\rho=1.0$  g/cm<sup>3</sup> the estimate

$$4.05 \cdot 10^{-3} < \chi'_{\text{max}} < 8.54 \cdot 10^{-3}$$

The calculated value of  $\chi'_{\text{max}}$ , namely  $6.77 \cdot 10^{-3}$ , falls in this interval.

From the known experimental values of the end points of the band in which the maximum value of  $\chi'(\omega)$  is located, we can calculate the corresponding values of the spectral density of radiation from carbon per electron:

$$0.17 < (dW/d\omega)_{\text{max}} < 0.35.$$

The calculated spectral density of the x-ray Čerenkov radiation is 0.28. We have thus experimentally confirmed the existence of x-ray Čerenkov radiation and measured the maximum value of the permittivity of carbon near the  $K$  edge of the photoeffect.

## 8. CONCLUSION

The foregoing theoretical calculation and the first albeit insufficiently complete experimental results show that Čerenkov radiation in the x-ray region of the spectrum is of interest primarily as a source of monochromatic radiation with tunable wavelength and with small angle divergence. The frequency can be tuned in a

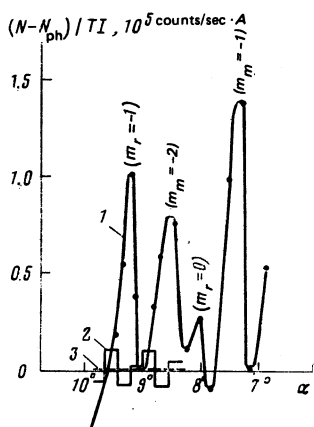


FIG. 7. Counting rate of x-ray photon as a function of the angle of rotation of the diffraction grating: 1) diffraction orders of the Čerenkov photons,  $m_r$ ) diffraction orders in the case of a ray path from the target through the diffraction grating to the detector;  $m_m$ ) diffraction orders in a ray path target-diffraction grating-mirror-detector; 2) spectrum of radiation from polyethylene target; 3) average value of the radiation spectrum from polyethylene target.

range of several electron volts by varying the observation angle. The monochromaticity of the x-ray Čerenkov radiation is close to that of x-ray tubes, and the directivity is close to that of synchrotron radiation.

Let us compare, for example, the spectral-angular density of Čerenkov and synchrotron radiation. According to the results of the theory of synchrotron radiation,<sup>27</sup> the spectral-angular energy density of the latter per electron does not exceed  $\approx 4.8 \cdot 10^{-4}$ . At the same time, for Čerenkov radiation we have in accordance with (22)

$$\left. \frac{d^2W}{d(h\omega)d\Omega} \right|_{\theta=0} \approx 7.4 \cdot 10^{-4} \frac{\chi' - \gamma^{-2}}{\chi''^n}$$

For a given particle energy  $E$  it is possible to choose the density of the medium such that this energy is equal to several times the threshold energy. Then, since  $\chi' \gg \chi''$  in the region of the Čerenkov frequencies, it turns out that the Čerenkov radiation has a substantially larger spectral-angular density than synchrotron radiation. Calculated per electron, the spectral-angular density of the Čerenkov radiation is comparable only with the corresponding value for an undulator<sup>28</sup> with  $N = (\chi')^{1/2}/\chi''$  periods.

It should be noted that the threshold for generation of soft x-rays in solids (Al, C) turns out to be relatively low (several MeV), while in undulators this calls for an energy of hundreds of MeV. It becomes possible therefore to obtain soft x-rays with the aid of small linear accelerators for such purposes as x-ray lithography, the investigation of the structure of the  $K$  photoeffect edge of organic compounds, and other problems. Interest attaches also to the investigation of stimulated Čerenkov radiation and to the problem of developing on this basis a laser operating in the soft x-ray and ultraviolet frequency bands.

<sup>1</sup>J. V. Jelley, Čerenkov Radiation, Pergamon, 1959.

<sup>2</sup>V. P. Zrellov, Izlučenie Vavilova-Cherenkova i ego primenenie v fizike vysokikh energiĭ (Vavilov-Cherenkov Radiation and Its Use in High-Energy Physics), Atomizdat, 1972.

<sup>3</sup>B. M. Bolotovskii, Usp. Fiz. Nauk **75**, 295 (1961) [Sov. Phys. Usp. **4**, 781 (1962)].

<sup>4</sup>M. A. Piestrup, R. A. Powell, G. B. Rothbart, C. K. Chen, and R. H. Pantell, Appl. Phys. Lett. **28**, 92 (1976).

<sup>5</sup>A. V. Kolpakov, Yad. Fiz. **16**, 1003 (1972) [Sov. J. Nucl. Phys. **16**, 554 (1973)].

<sup>6</sup>V. A. Bazylev, V. I. Glebov, É. I. Denisov, N. K. Zhevago, and A. S. Khlebnikov, Pis'ma Zh. Eksp. Teor. Fiz. **24**, 406 (1976) [JETP Lett. **24**, 371 (1976)].

<sup>7</sup>V. A. Bazylev, V. I. Glebov, É. I. Denisov, N. K. Zhevago, and A. S. Khlebnikov, Preprint IAE-2765, Kurchatov Atomic Energy Inst., 1977.

<sup>8</sup>V. V. Yakimets, in: Prokhozhdenie izlucheniya cherez veshchestvo (Penetration of Radiation Through Matter), Atomizdat, 1968, p. 106.

<sup>9</sup>V. E. Pafomov, Dokl. Akad. Nauk SSSR **213**, 819 (1973) [Sov. Phys. Dokl. **18**, 808 (1974)].

<sup>10</sup>V. A. Bazylev, A. A. Varfolomeev, and N. K. Zhevago, Zh. Eksp. Teor. Fiz. **66**, 464 (1974) [Sov. Phys. JETP **39**, 222 (1974)].

<sup>11</sup>P. Budini, Nuovo Cimento **10**, 236 (1953).

<sup>12</sup>V. V. Yakimets, Dokl. Akad. Nauk SSSR **159**, 728 (1964).

<sup>13</sup>N. K. Zhevago, Zh. Eksp. Teor. Fiz. **72**, 428 (1977) [Sov. Phys. JETP **45**, 224 (1977)].

<sup>14</sup>V. P. Silin, Vvedenie v kineticheskuyu teoriyu gazov (Introduction to the Kinetic Theory of Gases, Nauka, 1971, p. 115.

<sup>15</sup>E. M. Lifshitz and L. P. Pitaevskii, Relativistic Quantum Theory, part 2, Pergamon, 1974.

<sup>16</sup>E. Fermi, Phys. Rev. **57**, 458 (1940).

<sup>17</sup>G. M. Garibyan, Izv. AN SSSR, ser. Fiz. **26**, 754 (1962).

<sup>18</sup>V. G. Baryshevskii and Ngo Dan Nyang, Yad. Fiz. **20** (1974) [Sov. J. Nucl. Phys. **20**, 636 (1975)].

<sup>19</sup>G. M. Garibyan and Yang Shi, Pis'ma Zh. Eksp. Teor. Fiz. **24**, 269 (1976) [JETP Lett. **24**, 239 (1976)].

<sup>20</sup>G. M. Garibyan, Doctoral Dissertation Erevan, 1961.

<sup>21</sup>V. M. Samsonov, Zh. Eksp. Teor. Fiz. **75**, 88 (1978) [Sov. Phys. JETP **48**, 44 (1978)].

<sup>22</sup>B. W. Shore, Rev. Mod. Phys. **39**, 439 (1967).

<sup>23</sup>H. Hönl, Ann. Physik **18**, 538 (1933).

<sup>24</sup>W. J. Veigele, Atomic Data and Nucl. Data Tables, **5**, 51 (1973).

<sup>25</sup>J. H. Hubbell, Atomic Data and Nucl. Data Tables, **3**, 2 (1971).

<sup>26</sup>A. A. Sokolov and I. M. Ternov, Relyativistskiĭ élektron (The Relativistic Electron), Nauka, 1974.

<sup>27</sup>S. Krinski, IEEE Trans. Nucl. Sci. **26**, 73 (1979).

Translated by J. G. Adashko